Dual Alloying Strategy to Achieve a High Thermoelectric Figure of Merit and Lattice Hardening in p-Type Nanostructured PbTe

Sumanta Sarkar,[†] Xiaomi Zhang,[¶] Shiqiang Hao,[¶] Xia Hua,[¶] Trevor P. Bailey,[§] Ctirad Uher,[§] Chris Wolverton,[¶] Vinayak P. Dravid,[¶] and Mercouri G. Kanatzidis[*,†]
[†]Department of Chemistry, Northwestern University, Evanston, Illinois 60208, United States
[¶]Department of Materials Science and Engineering, Northwestern University, Evanston, Illinois 60208, United States
[§]Department of Physics, University of Michigan, Ann Arbor, Michigan 48109, United States

ABSTRACT:

The introduction of an alkaline earth metal telluride as a second phase in PbTe can lead to very high thermoelectric figure of merit, ZT, as a result of hierarchical structuring, e.g., in the PbTe−SrTe system. However, there are two roadblocks to this strategy: poor solubility and occurrence of incoherent nanoprecipitates in the PbTe matrix, e.g., the PbTe−BaTe system. Here we demonstrate a dual alloying approach by simultaneously alloying CaTe and BaTe in the p-type PbTe matrix to achieve ZTmax ranging up to ∼2.2 at high temperatures. Synergistic enhancement of the Seebeck coefficient via favorable band convergence gives rise to higher power factors up to 34 μW cm−1 K−2 and significant suppression of lattice thermal conductivity, κL, down to ∼0.6 W m−1 K−1 results from large multicenter phonon scattering. Additionally, co-inclusion of Ca and Ba causes unanticipated lattice hardening in otherwise brittle PbTe, essential for practical device applications.

A vast amount of energy is wasted in the form of heat, mainly through industrial machinery and automobiles.[1] Thermoelectric materials that can convert heat into electricity or vice versa have tremendous potential to utilize a certain portion of this waste heat for useful electrical energy.[2,3] The heat to electricity conversion efficiency of a material is characterized by the thermoelectric figure of merit, ZT, which incorporates both electrical and thermal transport properties of a material, and is expressed as $\sigma S^2T/\kappa$, where σ is the electrical conductivity, S is the Seebeck coefficient, κ is the total thermal conductivity, and T is the absolute temperature.4 The term σS^2 is known as the "power factor" (PF), and κ is a combination of the electrical (κ_e) and lattice contributions (κ_L). It is apparent from the above expression that an increase in PF or a decrease in κ will enhance the ZT. However, any attempt to increase the electrical conductivity of a material will inherently lead to an increase in κ_e as they are directly related by the Wiedemann− Franz law.[5,6]

Achieving a high PF demands a delicate balance between the mobility (μ) and effective mass (m*) of the carriers.[6−11] κ_L, on the other hand, depends on the inherent structural complexity, anharmonicity of the bonding, as well as micro/nanostructural details of a material.[10−16] A powerful technique to reduce the thermal conductivity and enhance the power factor is to introduce nanoscale precipitates in the bulk matrix for enhanced phonon scattering.[17] This method has been successfully applied to PbTe as well as other thermoelectric materials.[15,18−20]

Furthermore, an effective route to enhance ZT is by boosting the S, which can be achieved through the introduction of resonant impurity levels to increase the density of states (DOS) near the Fermi level[21] or by enhancing the band degeneracy by converging the heavy (Σ) and light (L) hole bands in PbTe, by alloying with certain metal tellurides,[22] e.g., MgTe,[10] SrTe (in both equilibrium and nonequilibrium processing),[7,11] MnTe,[23] CdTe,[24] YbTe,[25] etc. It was shown that by embedding endotaxial SrTe nanoscale precipitates with good valence band alignment in p-type PbTe, the heat flow could be significantly inhibited without affecting the hole carrier mobility to create an all-scale hierarchical system with a very high ZT.[7] A roadblock to further extend this approach to certain systems is the poor solubility of alkaline earth metal tellurides (MTe, M = Mg, Ca, Sr, Ba) in PbTe. In particular, attempts with PbTe−CaTe and PbTe−BaTe systems have not yielded such high ZT values (1.5 for Pb0.98Na0.02Te−6% CaTe at 765 K and 1.3 for Pb0.98Na0.02Te−3% BaTe at 760 K).[13]

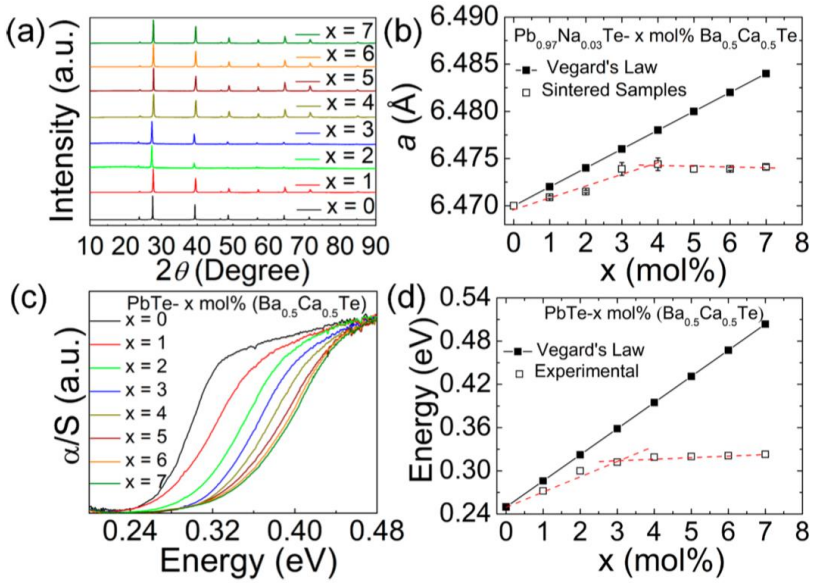

Figure 1. (a) PXRD patterns of sintered Pb0.97Na0.03Te with x mol % Ba0.5Ca0.5Te (x = 0−7). (b) Variation of the lattice parameters of PbTe−x mol % (Ba0.5Ca0.5Te). The cross-point suggests a solubility limit of ∼4 mol % for Ba0.5Ca0.5Te in PbTe. (c) Fourier transformed infrared (4000−400 cm−1) absorption spectra for PbTe−x mol % (Ba0.5Ca0.5Te) samples without Na doping. The spectra were collected in solid-state diffuse reflectance mode. α and S are the Kubelka−Munk absorption and scattering coefficient, respectively (see the SI for details). (d) Band gap enlargement of PbTe with increasing Ba0.5Ca0.5Te fraction; the cross-point indicates that the band gap enlargement saturates at ∼3−4 mol %.

In this work, we address this issue and show that the solubility of metal tellurides in a PbTe matrix can be enhanced by adopting a “dual alloying” strategy in which two separate second phases are incorporated at the same time. We demonstrate the effectiveness of this strategy in the case of a Na-doped PbTe−(BaTe)1−y(CaTe)y pseudoquaternary system. CaTe and BaTe were chosen in this work because they possess respectively smaller and larger lattice constants than PbTe itself; therefore, we hypothesized that a self-compensation effect may be

achieved to increase the solubility of the CaTe/BaTe mixture upon dual alloying. As a result the thermal conductivity is drastically reduced in PbTe by alloy scattering as well as nanostructuring (κ_L as low as ∼0.6 W m−1 K−1) process. In addition, the dual alloying significantly enhances the power factor, PF, reaching >30 μW cm−1 K−2 at around 600 K by decreasing the energy difference between the Σ and L bands, all of which contribute to achieve a state of the art thermoelectric figure of merit ZT_{max} of 2.2 at 823 K for PbTe−1 mol % (Ba0.5Ca0.5Te) doped with 3 mol % Na. Both the PF and ZT in the CaTe and BaTe dual-alloyed PbTe are among the highest reported for p-type PbTe systems.[7,10,11] The added benefit of the dual alloying in p-type PbTe−x mol % (Ba1−yCayTe) materials presented here is the improved lattice hardness properties that are necessary for the assembly of robust thermoelectric generators. This unanticipated improvement is due to the precipitation hardening effect, giving rise to significantly higher hardness over p-type PbTe, as well as single-alloyed PbTe−4% SrTe and nonequilibrium processed PbTe−8% SrTe.[26−28] The sintered PbTe−x mol % (Ba0.5Ca0.5Te), where x = 0−7, samples were screened using powder X- ray diffraction (PXRD) (Figure 1a). The main PXRD peak at 27.54° corresponding to the (200) plane in PbTe shifts toward lower angle with increasing x, indicating an overall expansion of the PbTe unit cell with the addition of "Ba0.5Ca0.5Te" up to x = 4 and then saturates beyond this point (Figure 1b). A small peak from a second phase, predominantly BaTe, begins to appear at 25.4° beyond composition x = 4 (Figure S1). It should be noted that this series of compounds does not completely follow Vegard's law (Figure 1b, black solid line), which can be explained by the fact that BaTe here acts as a "microalloying" phase because only a small fraction (<1 mol %) is soluble in PbTe. Because both second phases are wide-band-gap semiconductors, CaTe (4.4 eV) and BaTe (3.6 eV), it is expected that the band gap of PbTe after alloying would increase with their phase fraction (x).[13] The optical absorption data (Figure 1c) shows that the band gap does increase with increasing x and almost saturates beyond x = 4; again, the experimental data do not follow the trend predicted by the Vegard's law (Figure 1d). Both PXRD and optical band gap studies corroborate earlier literature that reported very poor solubility for BaTe in the PbTe matrix.[13,29] The rest of the added BaTe forms nanoprecipitates (Figure 2a,b). These precipitates are 50−500 nm wide. The precipitates are sparse and mostly located at grain boundaries in the Pb0.97Na0.03Te with 1 mol % Ba0.5Ca0.5Te sample, while a larger number of precipitates was observed both inside of the grains and at the grain boundaries for the 4 mol % Ba0.5Ca0.5Te alloyed sample. The precipitate densities for 1 and 4 mol % Ba0.5Ca0.5Te samples were roughly estimated to be 9.7 × 1018 and 3.8 × 1019/m^3, respectively.

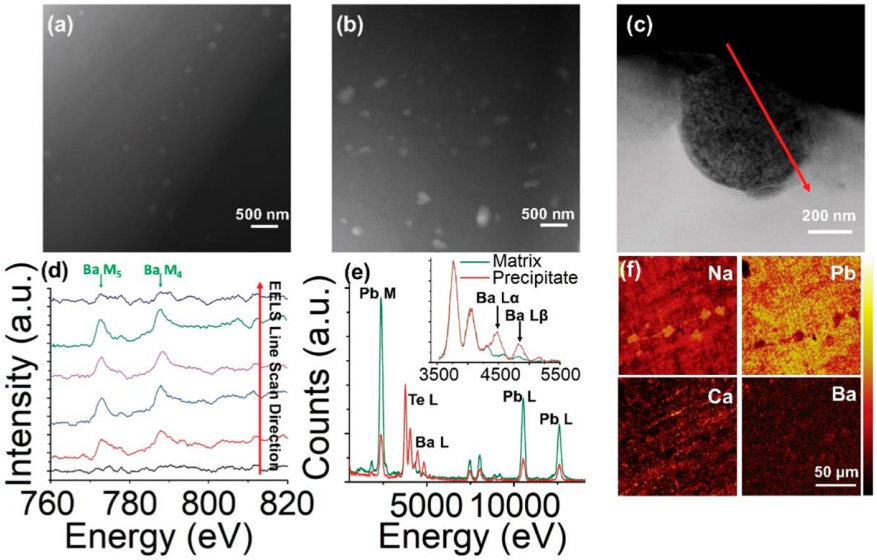

Figure 2. Annular dark field (ADF) STEM images of (a) Pb0.97Na0.03Te−1 mol % Ba0.5Ca0.5Te and (b) Pb0.97Na0.03Te−4 mol % Ba0.5Ca0.5Te. (c) HAADF STEM image of Pb0.97Na0.03Te−4 mol % Ba0.5Ca0.5Te. The red arrow indicates the EELS line scan location. (d) EELS line scan spectra of the region indicated by the red arrow in (c). (e) Representative EDS spectra of Pb0.97Na0.03Te−4 mol % Ba0.5Ca0.5Te, taken from both the matrix (green solid line) and nanoscale precipitate (red solid line). The inset spectra highlight differences in Ba L peak intensities. (f) SIMS element maps of Na, Pb, Ca, and Ba in Pb0.97Na0.03Te−1 mol % Ba0.5Ca0.5Te. The maps highlight the relative concentration distribution of each individual element. Note that the absolute intensities between elemental maps are not comparable due to different SIMS ionization cross sections.

Electron energy loss spectrum (EELS) line scanning on a nanoprecipitate showed that these are rich in BaTe (Figure 2c–e). EDS analysis further confirmed that the precipitates are rich in Ba and deficient in Pb. To obtain a better qualitative understanding of the relative Ba and Pb concentrations in the matrix and precipitates, the two spectra were normalized with respect to the Te Lα peak at 3769 eV. Figure 2e gives two representative spectra from the material matrix[30] and nanoscale precipitates (red). The spectrum from the precipitate shows stronger Ba peak intensities and weaker Pb peak intensities than the matrix, further confirming that the precipitates are Barich and Pb-deficient. The crystal structure of the nanoscale precipitates is further analyzed in Figure S2, where the fast Fourier transform (FFT) of the lattice fringes in the nanoscale precipitate shows it has a rock salt structure with a lattice parameter between that of PbTe and BaTe. This microalloyed BaTe, in turn, helps to increase the solubility of CaTe in PbTe. This is evident from the even distribution of Ca in the PbTe matrix (Figure 2f). The chemical composition of precipitates in the 4 mol % sample was then analyzed in detail with both EELS and EDS. EELS line scans were carried out along the line indicated by the red arrow in Figure 2c, and the corresponding spectra are shown in Figure 2d. Ba has an EELS M5 edge at 781 eV and M4 edge at 796 eV. EELS spectra obtained within the precipitate show clear Ba M edges, indicating that the precipitates are rich in barium. Secondary ion mass spectrometry (SIMS) elemental maps demonstrate that Ba and Ca also both exist in the matrix in the form of

solid solution. Figure 2f shows SIMS maps of Na, Pb, Ca, and Ba in the 1 mol % sample, indicating that Ba and Ca have relatively uniform distribution across the microscale. It is worth noting that Na segregation was observed at certain grains (Figure 2f) and at grain boundaries (Figure S3) according to SIMS. Wu et al. also observed similar Na segregation in a PbTe−PbS pseudobinary grain/phase boundary. They attributed the high electrical properties in their system to the redistribution of Na back into the PbTe matrix, leading to carrier modulation at higher temperature.[9]

Here, we must point out that CaTe and BaTe by themselves are hardly soluble in PbTe, as previously reported by Biswas et al.[13] The poor solubility of CaTe in the PbTe matrix (in the absence of BaTe) is evident from the fact that the lattice parameter and band gap of PbTe remain almost unchanged with the addition of CaTe. In order to prove this point, we synthesized a series of control samples, PbTe−x mol % CaTe, and measured the change in lattice parameter and band gap of PbTe with increasing CaTe content (Figures S4 and S5). It is evident from Figures S4b and S5b that the changes in both parameters are quite negligible, and hence, it can be concluded that CaTe in the absence of BaTe is hardly soluble. However, microalloying a small amount of BaTe (6.999 Å) in PbTe (6.471 Å) will lead to expansion of the PbTe lattice, which in turn may facilitate enhanced solubility of CaTe (6.350 Å) to balance the tensile (expansion) and compressive (shrinking) strains. This is similar to what is done in metal alloying where, for example, alloying a small amount of molybdenum enhances the solubility of other trace elements in steel.[31]

The PbTe−x mol % (Ba0.5Ca0.5Te) (x = 0−5) samples were initially doped with 2 mol % Na. The thermoelectric properties of x = 6 and 7 were not measured as there was significant phase separation of bulk BaTe observed in the PXRD patterns (Figure S1). The measured room-temperature electrical conductivity (σ) decreased monotonically as a function of x from 2279 S cm−1 for the unalloyed sample to 1743 S cm−1 for x = 1 and to a minimum of 1491 S cm−1 at the 5 mol % (Ba0.5Ca0.5Te) level, as shown in Figure S6a and listed in Table S2. The room-temperature Seebeck coefficient (S) behaves in the opposite manner, with values of 62, 70, and 92 μV K−1 for x = 0, 1 and 5, respectively; see Figure S6b. Interestingly, the electrical conductivities are relatively lower than those of the analogous Pb0.98Na0.02Te−x mol % SrTe series of compounds with similar x values reported by Tan et al.11 In order to understand the reason behind the difference, we measured the room-temperature carrier concentrations in the 2 mol % Nadoped samples, which range from 7−9 × 1019 cm−3 (see Table S2) and are relatively lower than the corresponding Pb0.98Na0.02Te−SrTe analogues (nH = 1.4−1.7 × 1020 cm−3).11 To achieve higher hole concentration in PbTe−x mol % (Ba0.5Ca0.5Te), the dopant (Na) concentration was increased to 3 mol %. The higher Na doping levels resulted in considerably enhanced electrical conductivity throughout the whole series of samples (Figure 3a).

For example, the room-temperature electrical conductivity of Pb0.97Na0.03Te (3051 S cm−1) is much higher than that of Pb0.97Na0.02Te (2280 S cm−1). The rest of the data is shown in Figure 3. It is clear from Figure 3a and Table 1 that the room- temperature electrical conductivity decreases with x in Pb0.97Na0.03Te−x mol % (Ba0.5Ca0.5Te) mainly due to decreasing carrier mobility (Figure 3d), which is compensated by the increasing Seebeck coefficients (Figure 3c) as a result of the increasing DOS effective mass, mDOS* (Figure 3d).

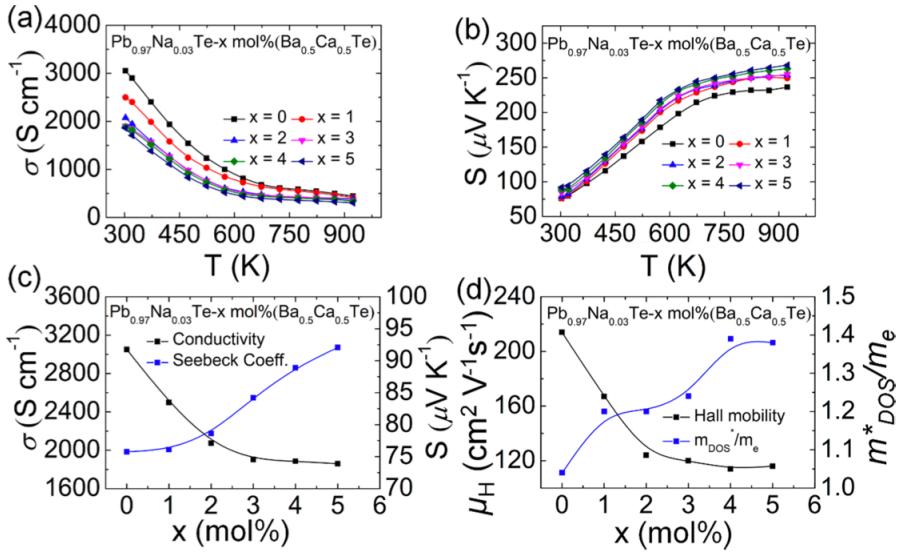

Figure 3. Variation of the (a) electrical conductivity and (b) Seebeck coefficient with temperature; effect of composition (x mol %) on the (c) room-temperature electrical conductivity and Seebeck coefficient (d) Room temperature Hall mobility and DOS effective mass (mDOS*) for Pb0.97Na0.03Te−x mol % Ba0.5Ca0.5Te (x = 0−5).

Table 1. Room-Temperature (300 K) Electrical Transport Properties of Pb0.97Na0.03Te−x% (Ba0.5Ca0.5Te)

x	σ (S cm^{-1})	S (μV K^{-1})	n_H (10^{20} cm^{-3})	μ_H (cm^2 V^{-1} s^{-1})	m_{DOS}*/m_e
0	3051	75.7	1.42	134	1.04
1	2498	76.0	1.73	90	1.19
2	2073	78.6	1.67	77	1.20
3	1902	84.2	1.58	75	1.24
4	1885	88.9	1.65	71	1.35
5	1850	92.0	1.61	72	1.38

Note that the carrier concentration does not change drastically in this series of compounds (Table 1); hence, the most probable reason for the reduced carrier mobility is the redistribution of holes in the heavy valence band (Σ- band) that yields an overall larger mDOS* as a result of the broadened Fermi distribution.[8] The closing of the gap between the two bands is generally referred to as “band convergence”.[10,22,32,33] The occurrence of band convergence can be probed by measuring the temperature-dependent Hall coefficient, RH. For semiconductors that feature a typical single-band carrier transport, the RH is almost invariant with temperature.[34] However, when electronic transport occurs in more than one band, the temperature-dependent redistribution of holes in the light and heavy hole bands with different mobilities leads to RH values that vary considerably with temperature. In the case of p-type

PbTe, a maximum in RH occurs at around 425 K.[33] It has been previously observed that the peak temperature for RH significantly shifts to lower temperature in the cases of Pb(1−x)MxTe (M = Mn, Cd, Mg, Sr, and Yb), suggesting that such alloying further assists in valence band convergence. A similar trend was observed in the case of Pb0.97Na0.03Te−x mol % Ba0.5Ca0.5Te, (x = 1, 2, and 4), which indicates narrowing of the gap between the light (L) and heavy (Σ) bands; see Figure 4a.

The temperature-dependent Hall mobility, μ_H, for Pb0.97Na0.03Te−x mol % Ba0.5Ca0.5Te, (x = 1, 2, and 4) is shown in Figure 4b. The room-temperature μH values for these three systems were found to be ∼90, ∼77, and ∼71 cm2 V−1 s−1 (Table 1), respectively. These values are lower than those of the pristine Pb0.97Na0.03Te sample (134 cm2 V−1 s−1, Table 1) but higher than or comparable to those of previously reported alloyed PbTe-based systems that show band convergence, such as Na:Pb0.97Mn0.03Te (65 cm2 V−1 s−1),[23] Na:Pb0.97Mg0.03Te (69 cm2 V−1 s−1), Na:Pb0.92Sr0.04Mn0.04Te (62 cm2 V−1 s−1), Na:Pb0.98Sr0.02Te (78 cm2 V−1 s−1), etc. This can be explained based on the larger size difference in the size of Pb2+ (1.19 Å) compared to Mn2+ (0.81 Å) and Mg2+ (0.86 Å), giving rise to stronger electron scattering in these systems. On other hand, Ca2+ (1.14 Å) and Sr2+ (1.32 Å) have similar size; hence, the electron scattering by the lattice defects is much less pronounced.[7,11,35] μH follows a power law (Tδ) throughout the entire measured temperature range. In the low temperature range (294−425 K), μH varies as T−1.5, indicating that the carrier scattering is dominated by acoustic phonon scattering, whereas in the high-temperature range, $\mu H \propto T^{-3.25}$, which is normally attributed to increasing effective mass as a function of temperature. This supports the idea of band convergence as the carriers are redistributed from the light L band into the heavy Σ band. The valence band convergence achieved by Ba0.5Ca0.5Te alloying effectively gives rise to enhancement of the S. This is depicted in Figure S12 by the Pisarenko relation between S and n. It can be seen that the S values for our (Ba0.5Ca0.5Te)-alloyed PbTe samples are situated above the predicted solid line for PbTe. This, in turn, is reflected in the overall PF of the samples (Figures 4d and S13). The redistribution of carriers to heavy hole bands (e.g., Σ band) should effectively increase the DOS effective mass (mDOS*). In order to get a reasonable estimate, we calculated the room-temperature DOS carrier effective mass (mDOS*) of each sample from the experimentally measured S and n considering a single parabolic band (SPB) model8 for the sake of simplicity. It can be seen in Table 1 that the mDOS* rises from 1.04me to 1.37me (me being the free electron mass, 9.11×10^{-31} kg) with increasing Ba0.5Ca0.5Te content from 0 to 5 mol %. As shown above, alloying with Ba0.5Ca0.5Te brings the L and Σ valence band tops closer in energy. Because the band degeneracy (Nv) of the Σ band is very high (Nv = 12) compared to the L band (Nv = 4), the DOS effective mass is enhanced, owing to the following relation

$$m^*_{DOS} = (N_v)^{\frac{2}{3}} m^*_b \qquad (1)$$

where m_b* is the average band mass. A comparative analysis of the first-principles electronic band structure calculations considering spin−orbit coupling (Figure 4c) on Pb27Te27, Pb26CaTe27, and Pb26BaTe27 to Pb25BaCaTe27 (27 × 27 × 27 supercells) reveals that the light (L) and heavy (Σ) hole bands are indeed closest in the case of Pb25BaCaTe27 (ΔEL−Σ = 0.06 eV) in comparison to pristine Pb27Te27 (ΔEL−Σ = 0.14 eV). The corresponding value for Pb26CaTe27

and Pb26BaTe27 is 0.13 eV. Additionally, the predicted band gap for Pb25BaCaTe27 (Eg = 0.22 eV) is much larger than those for pristine Pb27Te27 (Eg = 0.10 eV) and Pb26CaTe27 (Eg = 0.06 eV) or Pb26BaTe27 (Eg = 0.08 eV). These predictions match well with the trend of the experimentally measured band gaps (Figures 1c and S11b). A high band gap helps suppress the bipolar conduction. Figure S14 shows the electronic DOS of Te atoms in three cases, including Ca, Ba, and Ca/Ba coalloyed system. For the single Ca or Ba alloyed PbTe, the 5p electronic states of neighboring Te atoms are not affected significantly. Thus, the Σ band position hardly changes relative to pure PbTe (Figure 4c). However, for the Ca and Ba coalloyed case, due to significant atomic size difference, the two atoms prefer to stay in the first nearest neighbors, which affects the neighboring Te to a large extent. As a result, the 5p electronic states of neighboring Te atoms are significantly affected, which induces the Σ band position to be higher than the single alloyed or pristine PbTe systems.

Solely achieving optimal dopant concentration can ensure a high PF (and a high thermoelectric performance). This is evident by the fact that a high PF (26−30 μW cm−1 K−2, 525− 550 K) leading to high ZT (∼1.4 at ∼750 K) was previously reported by solely optimizing the carrier concentration to the higher end (∼9 × 10^{19} cm−3) in Na-doped PbTe, without introducing any other metal telluride as a second phase.[8,36] The optimal carrier concentration combined with highly efficient band convergence, discussed above, gives even higher power factors in the Pb0.97Na0.03Te−x mol % (Ba0.5Ca0.5Te) samples (Figure 4d), with the maximum values in the range of 30−34 μW cm−1 K−2 at around 600 K. For example, the 1 mol % Ba0.5Ca0.5Te-containing sample displays a significantly higher PF than Na-doped PbTe alloyed with 3 mol % MgTe, MnTe, and SrTe (Figure S13).[10,11,23] These values are among the highest reported for p-type PbTe.[11]

It is also worthwhile to compare the temperature-dependent PF of 2 and 3 mol % Na-doped PbTe−x mol % Ba0.5Ca0.5Te (Figures 4d and S6c). In the case of 2 mol % Na-doped samples, the effect of Ba0.5Ca0.5Te alloying in PbTe is quite apparent with the room-temperature PF increasing from 9.5 μW cm−1 K−2 for x = 0 to 11.4 μW cm−1 K−2 for x = 2, 12.5 μW cm−1 K−2 for x = 3, 12.7 μW cm−1 K−2 for x = 4, and 12.7 μW cm−1 K−2 for x = 5 (Figure S6c). The maximum PF achieved is ∼30 μW cm−1 K−2 for x = 3 at 575 K. In the case of 3 mol % Na-doped PbTe−x mol % Ba0.5Ca0.5Te samples, the above trend is not apparent as the PF at room temperature is highest for x = 0, i.e., Pb0.97Na0.03Te (17.5 μW cm−1 K−2, Table S2 and Figure 4d). The corresponding room-temperature PF values for x= 1−5 in this series of samples are 14.4, 12.8, 13.4, 15.8, and 15.7 μW cm−1 K−2, respectively. This apparent discrepancy can be understood by the competing effects of carrier mobility and effective mass. Pb0.97Na0.03Te (i.e., x = 0) has the highest carrier mobility (134 cm2 V−1 s−1) among these samples (x = 0−5), leading to a very high electrical conductivity (3051 S cm−1) that dominates the PF. The electrical conductivity for samples with x = 1−5 falls almost exponentially due to a decrease in carrier mobility (Figure 3c,d). As seen in Figure 3c,d, the negative impact of decreasing electrical conductivity and carrier mobility is countered by an increasing Seebeck coefficient and effective mass with x. As a result, the maximum PF in these samples (x = 1−5) ranges from 25 to 34 μW cm−1 K−2 in the temperature range of 573− 623 K. However, it is important to stress that the highest change in carrier mobility occurs from x = 0 (i.e., pristine Pb0.97Na0.03Te) to x = 1 (134−90 cm2 V−1 s−1) because the BaTe-rich nanoprecipitates start to form at this stage. With increasing Ba0.5Ca0.5Te fraction, the number density of these nanoprecipitates increases, as

can be seen in Figure 2a,b. Because these nanoprecipitates are semicoherent, the carrier mobility is not interrupted to a great extent even though their number density increases. This is also manifested in the corresponding electrical conductivity (σ) data. The greatest drop in σ for Pb0.97Na0.03Te−x mol % Ba0.5Ca0.5Te occurs from x = 0 to 1 and 2 (3051 S cm−1 to 2498 and 2073 S cm−1; see Table 1). Thereafter, the drop in σ is not significant. This is further boosted by the fact that, unlike many other Na-doped p-type PbTe systems, the Seebeck coefficient in the PbTe−x mol % Ba0.5Ca0.5Te series of samples neither saturates nor falls down at temperature > 600 K. This is perhaps due to the fact that the presence of both Ca and Ba in the PbTe matrix does not allow the excess sodium locked in the grain boundaries to dissolve back into the grains.[9]

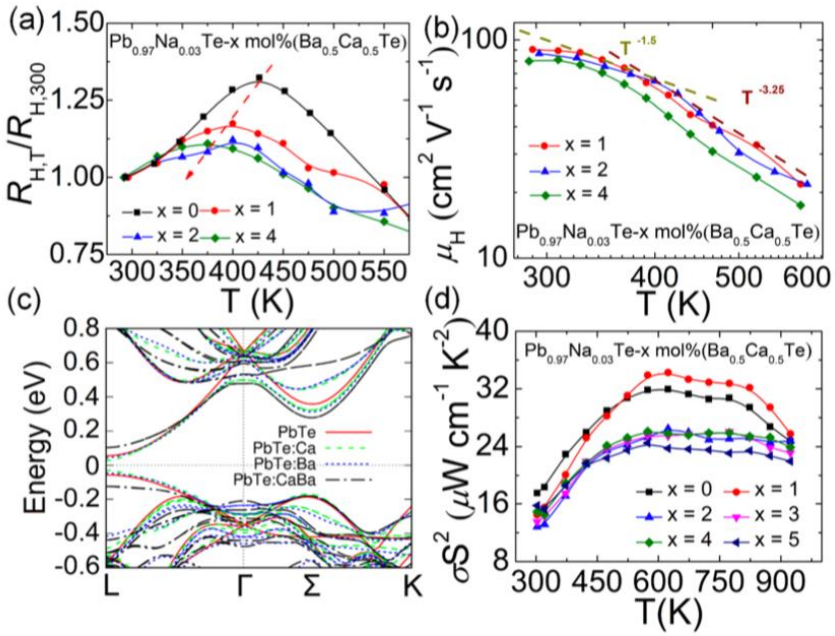

Figure 4. Temperature-dependent (a) Hall coefficient (normalized against the room-temperature value) and (b) Hall mobility data (plotted in log−log scale). The mobility follows a power law (Tδ) with the power continuously changing with temperature due to the transition to the heavy hole valence band transport. (c) First-principles band structure calculations for Pb27Te27 (red, solid), Pb26CaTe27 (green, dashed), Pb26BaTe27 (blue, dotted), and Pb25BaCaTe27 (black, dash−dot). Spin−orbit interaction (SOI) is included. (d) Temperature-dependent power factor (σS2) for Pb0.97Na0.03Te−x mol % Ba0.5Ca0.5Te samples (x = 0−5).

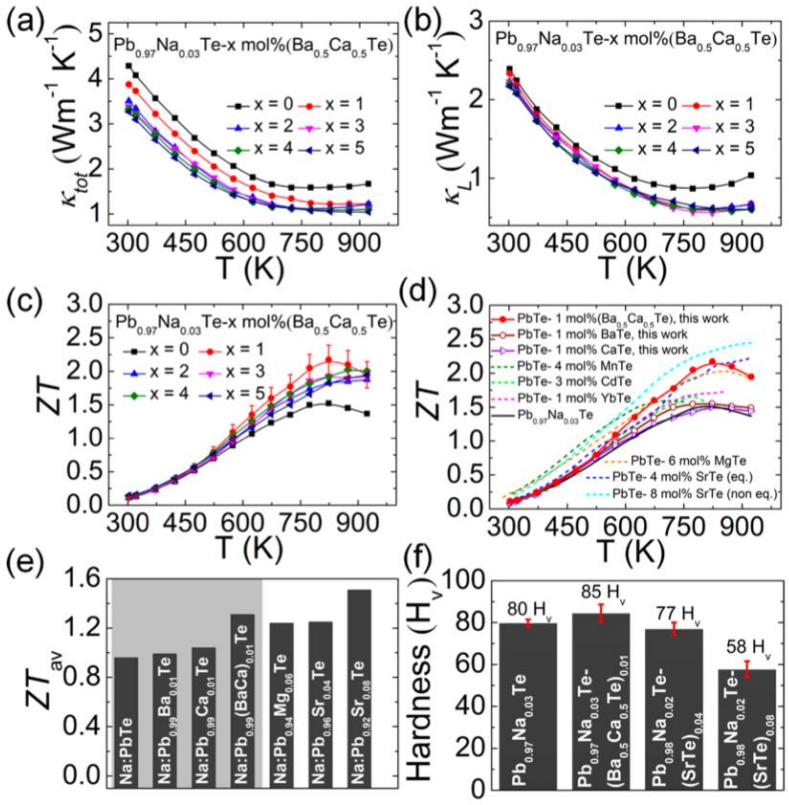

Figure 5. (a,b) Total and lattice thermal conductivity for Pb0.97Na0.03Te−x mol % Ba0.5Ca0.5Te (x = 0−5). (c) Temperature-dependent ZT of Pb0.97Na0.03Te−x mol % (x = 0−5) Ba0.5Ca0.5Te. (d) Comparison of ZT values for samples studied in this work (Pb0.97Na0.03Te−1 mol % MTe, M = Ba, Ca, and Ba0.5Ca0.5Te) with literature.7,10,11,23,24 (e) Comparison of ZT_{av} of Pb0.97Na0.03Te−1 mol % MTe, M = Ba, Ca, and Ba0.5Ca0.5Te (shaded) with literature data in the range of 300−900 K. (f) Microhardness (in Vicker's scale, Hv) of Pb0.97Na0.03Te−x mol % Ba0.5Ca0.5Te (x = 0 and 1), Pb0.98Na0.02Te−4 mol % SrTe (eq.), and Pb0.98Na0.02Te−8 mol % SrTe (non eq.) against a load of 0.2 kg-force for 10 s. The error bars represent the standard deviation over 10 measured data points.

The total thermal conductivity (κ_{tot}) of the Pb0.98/0.97Na0.02/0.03Te−x mol % (Ba0.5Ca0.5Te), x = 0−5, samples decreases with increasing x (Figures 5a and S6e). In order to understand the effect of Ba0.5Ca0.5Te alloying in PbTe, the corresponding temperature-dependent lattice thermal conductivities, κ_L, were calculated using the Lorenz numbers (see the Supporting Information). The room-temperature κ_L derived from the above analysis of Pb0.97Na0.03Te−x mol % (Ba0.5Ca0.5Te), x = 0−5, decreases with x (Figure 5b and Table S2) and even more so at high temperatures. The main reason for the separation at high temperatures is that the bipolar conduction due to thermally excited electrons is suppressed in the (Ba0.5Ca0.5Te) alloyed PbTe system in comparison to the control (Pb0.97Na0.03Te). κ_L in PbTe and related compounds is mainly attributed to the Umklapp phonon−phonon scattering and phonons scattered by point defects generated by the alloying effect.[7,10,11,37] The effectiveness of the two scattering processes is determined by their corresponding relaxation

times, τ_U and τ_{PD}, respectively. A high relaxation rate (τ^{-1}), in general, will essentially translate into lower κ_L. The isovalent substitution of Pb with Ca and Ba drastically enhances the phonon scattering (manifested by a high relaxation rate, τ_{PD}^{-1} eq 2) due to significant mass difference (Pb: 207.2 g mol−1; Ba: 137.327 g mol−1; Ca: 40.078 g mol−1) as well as the considerable strain between the host matrix and alloyed atoms of different ionic radii (Pb^{2+}: 1.33 Å; Ba^{2+}: 1.49 Å; Ca^{2+}: 1.14 Å).[38]

$$\tau_{\mathrm{PD}}^{-1} \propto \left[\sum_{i=1}^{n}\left(1-\frac{M_i}{M}\right)^2+\sum_{i=1}^{n}\left(1-\frac{r_i}{r}\right)^2\right] \qquad (2)$$

where M_i and r are the mass and radii of the i^{th} atom and M and r are the average atomic mass and radii of all atoms in the unit cell. It has recently been shown that lattice expansion by alloying BaTe (6.990 Å) with PbTe (6.471 Å) gives rise to significant static strain in the PbTe lattice. As a result, the transverse optical (TO) phonon modes soften along the Γ point in the Brillouin zone and overlap destructively with acoustic phonon modes, leading to an additional reduction in κ_L.[27] Furthermore, phonon scattering by nanostructures contributes to the overall decrease in κ_L. Although small nanostructures (10 nm or smaller) are believed to be very effective in scattering phonons with small mean free paths (<10 nm) at room temperature,[39] by the fact that the ZT of the PbTe-based systems maximizes at relatively high temperature (>600 K), we expect that larger nanostructures play an important role in suppressing κ_L at higher temperature. The small nanostructures (5−10 nm) may dissolve in the matrix at high temperature, whereas larger nanostructures (∼ 50−100 nm) are predicted to be stable.[14,39,40] Finally, the mesoscale structuring created by the SPS processing further contributes in the scattering of long-wavelength phonons.[7]

The temperature-dependent thermoelectric ZT is shown in Figure 5c. The highest ZT achieved was ∼2.2 at 823 K for the Pb0.97Na0.03Te−1 mol % Ba0.5Ca0.5Te, which is highly reproducible (Figure S15) and stable over successive heating−cooling cycles (Figure S16). This value is significantly (∼ 46%) higher than the control Pb0.97Na0.03Te (ZT = 1.5 at 773 K, Figure 5c) as well as Pb0.97Na0.03Te−1 mol % BaTe (ZT = 1.6 at 823 K, Figure S18) and Pb0.97Na0.03Te−1 mol % CaTe (ZT = 1.5 at 823 K, Figure S18) with a similar doping level (∼1 × 1020 cm−3) and comparable to many other metal telluride alloyed PbTe systems, such as PbTe−4 mol % SrTe, PbTe−6 mol % MgTe, etc. (Figure 5d). High ZT values (1.9− 2.0) were also achieved for samples with larger fractions of Ba0.5Ca0.5Te in the temperature range of 873−923 K (Figure 5c). This further underscores the positive impact of the dual alloying strategy on the thermoelectric properties of PbTebased materials adopted in this work.

In order for these materials to be viable in thermoelectric device fabrication, they must exhibit a high average ZT, $ZT_{avg} = \left(\frac{1}{\Delta T}\int_{300}^{900} Z(T)\,dT\right)T_{avg}$ and good mechanical properties.[41,42] The average ZT of Pb0.97Na0.03Te−1 mol % (Ba0.5Ca0.5Te) was calculated to be ∼1.31 in the range of 300−900 K, much higher than Na-doped PbTe (ZTav = 0.95) and comparable to other group 2 metal telluride alloyed PbTe-based systems (Figure 5e). To our knowledge, only Pb0.98Na0.02Te−8 mol % SrTe shows a higher ZTav of 1.67 in the same temperature range. However, it should be noted that the incorporation of a high mol % of other metal tellurides into the PbTe matrix may adversely affect the mechanical properties, rendering them

susceptible to cracking during materials processing steps, e.g., lapping and dicing. To study the effect of alloying on the mechanical properties of PbTe, microhardness tests were performed in selected polycrystalline SPSed samples of this work (Figure 5f). We observed that Pb0.97Na0.03Te−1 mol % Ba0.5Ca0.5Te has a Vicker's hardness constant, Hv of 85 kg mm−2, which is higher than that of Pb0.97Na0.03Te (Hv = 80 kg mm−2), Pb0.97Na0.03Te−4 mol % SrTe (Hv = 77 kg mm−2), and nonequilibrium synthesized Pb0.97Na0.03Te−8 mol % SrTe (Hv = 58 kg mm−2) samples (Figure 5d). The reason for better mechanical properties in Pb0.97Na0.03Te−1 mol % Ba0.5Ca0.5Te compared to those for similar systems could be lattice and precipitation hardening due to low metal telluride content and better grain refinement.[26,43] Direct evidence of the lattice hardening comes from the increase in microhardness with increasing Ba0.5Ca0.5Te fraction in the Pb0.97Na0.03Te matrix (Figure S19). BaTe-rich semicoherent precipitates may further aid in blocking dislocation movement across the grain boundaries.[28,44,45]

In conclusion, the dual alloying approach for PbTe adopted in this study, where two different but isostructural phases are incorporated, is effective in improving the thermoelectric properties in two ways. First, the enhanced solubility of the CaTe achieved in the presence of BaTe gives rise to widening of the band gap and good convergence between the L and Σ bands, leading to high Seebeck coefficients with record-high PFs. Additionally, the point defects generated by the alloying, along with the BaTe-rich nanostructures, help in reducing the lattice thermal conductivity of the system. This synergistic approach yields a high ZT of ∼2.2 at 823 K in the Pb0.97Na0.03Te−1 mol % Ba0.5Ca0.5Te sample. The relatively low metal telluride content and small grain size jointly help in achieving superior hardness, which is essential for good machinability relevant for practical device applications. These results point to a new path toward improving the thermoelectric and mechanical properties in all-scale hierarchical PbTe-based materials by simultaneous addition of two isostructural second phases with substantially different lattice parameters.

ACKNOWLEDGMENTS

This work was supported by the Department of Energy, Office of Science Basic Energy Sciences under grant DE-SC0014520, DOE Office of Science. This work made use of the NUFABCOOK and MatCI Facilities which receive support from the MRSEC Program (NSF DMR- 1720139) of the Materials Research Center at Northwestern University. This work also made use of EPIC (JEOL 2100F TEM, Hitachi HD-2300 Dual EDS Cryo STEM, Fischione Model 1050 TEM Mill, and PHI TRIFT III ToF-SIMS) facility of Northwestern University's NUANCE Center, which has received support from the Soft and Hybrid Nanotechnology Experimental (SHyNE) Resource (NSF ECCS-1542205); the MRSEC program (NSF DMR-1720139) at the Materials Research Center; the International Institute for Nanotechnology (IIN); the Keck Foundation; and the State of Illinois, through the IIN. Temperature-dependent Hall measurements were supported by the U.S. Department of Energy, Office of Science, and Office of Basic Energy Sciences under Award Number DE-SC-0008574.

REFERENCES

(1) Zhang, Y. Thermoelectric Advances to Capture Waste Heat in Automobiles. ACS Energy Lett. 2018, 3 (7), 1523−1524.

(2) Dresselhaus, M. S.; Thomas, I. L. Alternative Energy Technologies. Nature 2001, 414 (6861), 332−337.

(3) DiSalvo, F. J. Thermoelectric Cooling and Power Generation. Science 1999, 285 (5428), 703−706.

(4) Goldsmid, H. J. Applications of Thermoelectricity; Methuen: London, 1960.

(5) Chester, G. V.; Thellung, A. The Law of Wiedemann and Franz. Proc. Phys. Soc., London 1961, 77 (5), 1005.

(6) Tan, G.; Hao, S.; Hanus, R. C.; Zhang, X.; Anand, S.; Bailey, T. P.; Rettie, A. J. E.; Su, X.; Uher, C.; Dravid, V. P.; et al. High Thermoelectric Performance in SnTe−AgSbTe2 Alloys from Lattice Softening, Giant Phonon−Vacancy Scattering, and Valence Band Convergence. ACS Energy Lett. 2018, 3 (3), 705−712.

(7) Biswas, K.; He, J.; Blum, I. D.; Wu, C.-I.; Hogan, T. P.; Seidman, D. N.; Dravid, V. P.; Kanatzidis, M. G. High-performance Bulk Thermoelectrics with All-scale Hierarchical Architectures. Nature 2012, 489 (7416), 414−418.

(8) Pei, Y.; LaLonde, A.; Iwanaga, S.; Snyder, G. J. High Thermoelectric Figure of Merit in Heavy Hole Dominated PbTe. Energy Environ. Sci. 2011, 4 (6), 2085−2089.

(9) Wu, D.; Zhao, L.-D.; Tong, X.; Li, W.; Wu, L.; Tan, Q.; Pei, Y.; Huang, L.; Li, J.-F.; Zhu, Y.; et al. Superior Thermoelectric Performance in PbTe-PbS Pseudo-binary: Extremely Low Thermal Conductivity and Modulated Carrier Concentration. Energy Environ. Sci. 2015, 8 (7), 2056−2068.

(10) Zhao, L. D.; Wu, H. J.; Hao, S. Q.; Wu, C. I.; Zhou, X. Y.; Biswas, K.; He, J. Q.; Hogan, T. P.; Uher, C.; Wolverton, C.; et al. Allscale Hierarchical Thermoelectrics: MgTe in PbTe Facilitates Valence Band Convergence and Suppresses Bipolar Thermal Transport for High Performance. Energy Environ. Sci. 2013, 6 (11), 3346−3355.

(11) Tan, G.; Shi, F.; Hao, S.; Zhao, L.-D.; Chi, H.; Zhang, X.; Uher, C.; Wolverton, C.; Dravid, V. P.; Kanatzidis, M. G. Non-equilibrium Processing Leads to Record High Thermoelectric Figure of Merit in PbTe−SrTe. Nat. Commun. 2016, 7, 12167.

(12) Sharma, S.; Schwingenschlögl, U. Thermoelectric Response in Single Quintuple Layer Bi2Te3. ACS Energy Lett. 2016, 1 (4), 875− 879.

(13) Biswas, K.; He, J.; Wang, G.; Lo, S.-H.; Uher, C.; Dravid, V. P.; Kanatzidis, M. G. High Thermoelectric Figure of Merit in Nanostructured p-type PbTe-MTe (M = Ca, Ba). Energy Environ. Sci. 2011, 4 (11), 4675−4684.

(14) Pei, Y.; Heinz, N. A.; LaLonde, A.; Snyder, G. J. Combination of Large Nanostructures and Complex Band Structure for High Performance Thermoelectric Lead Telluride. Energy Environ. Sci. 2011, 4 (9), 3640−3645.

(15) Hsu, K. F.; Loo, S.; Guo, F.; Chen, W.; Dyck, J. S.; Uher, C.; Hogan, T.; Polychroniadis, E. K.; Kanatzidis, M. G. Cubic
AgPbmSbTe2+m: Bulk Thermoelectric Materials with High Figure of Merit. Science 2004, 303 (5659), 818−821.

(16) Chang, C.; Wu, M.; He, D.; Pei, Y.; Wu, C.-F.; Wu, X.; Yu, H.; Zhu, F.; Wang, K.; Chen, Y.; et al. 3D Charge and 2D Phonon Transports Leading to High Out-of-Plane ZT In n-Type SnSe Crystals. Science 2018, 360 (6390), 778−783.

(17) Singh, D. J.; Terasaki, I. Thermoelectrics: Nanostructuring and More. Nat. Mater. 2008, 7 (8), 616−617.
(18) Bux, S. K.; Blair, R. G.; Gogna, P. K.; Lee, H.; Chen, G.; Dresselhaus, M. S.; Kaner, R. B.; Fleurial, J.-P. Nanostructured Bulk Silicon as an Effective Thermoelectric Material. Adv. Funct. Mater. 2009, 19 (15), 2445−2452.
(19) Fu, C.; Bai, S.; Liu, Y.; Tang, Y.; Chen, L.; Zhao, X.; Zhu, T. Realizing High Figure of Merit in Heavy-band p-type Half-Heusler Thermoelectric Materials. Nat. Commun. 2015, 6, 8144.
(20) Poudel, B.; Hao, Q.; Ma, Y.; Lan, Y.; Minnich, A.; Yu, B.; Yan, X.; Wang, D.; Muto, A.; Vashaee, D.; et al. High-thermoelectric Performance of Nanostructured Bismuth Antimony Telluride Bulk Alloys. Science 2008, 320 (5876), 634−638.
(21) Heremans, J. P.; Jovovic, V.; Toberer, E. S.; Saramat, A.; Kurosaki, K.; Charoenphakdee, A.; Yamanaka, S.; Snyder, G. J. Enhancement of Thermoelectric Efficiency in PbTe by Distortion of the Electronic Density of States. Science 2008, 321 (5888), 554−557.
(22) Pei, Y.; Wang, H.; Snyder, G. J. Band Engineering of Thermoelectric Materials. Adv. Mater. 2012, 24 (46), 6125−6135.
(23) (a) Pei, Y.; Wang, H.; Gibbs, Z. M.; LaLonde, A. D.; Snyder, G. J. Thermopower Enhancement in Pb1-xMnxTe Alloys and Its Effect on Thermoelectric Efficiency. NPG Asia Mater. 2012, 4, e28. (b) Tan, G. J.; Shi, F. Y.; Hao, S. Q.; Chi, H.; Bailey, T. P.; Zhao, L. D.; Uher, C.; Wolverton, C.; Dravid, V. P.; Kanatzidis, M. G. Valence Band Modification and High Thermoelectric Performance in SnTe Heavily Alloyed with MnTe. J. Am. Chem. Soc. 2015, 137 (35), 11507−11516.
(24) (a) Pei, Y.; LaLonde, A. D.; Heinz, N. A.; Snyder, G. J. High Thermoelectric Figure of Merit in PbTe Alloys Demonstrated in PbTe−CdTe. Adv. Energy Mater. 2012, 2 (6), 670−675. (b) Tan, G. J.; Shi, F. Y.; Hao, S. Q.; Chi, H.; Zhao, L. D.; Uher, C.; Wolverton, C.; Dravid, V. P.; Kanatzidis, M. G. Codoping in SnTe: Enhancement of Thermoelectric Performance through Synergy of Resonance Levels and Band Convergence. J. Am. Chem. Soc. 2015, 137 (15), 5100− 5112.
(25) Jian, Z.; Chen, Z.; Li, W.; Yang, J.; Zhang, W.; Pei, Y. Significant Band Engineering Effect of YbTe for High Performance Thermoelectric PbTe. J. Mater. Chem. C 2015, 3 (48), 12410−12417.
(26) Zhang, Y.; Wu, L.; Zhang, J.; Xing, J.; Luo, J. Eutectic Microstructures and Thermoelectric Properties of MnTe-Rich Precipitates Hardened PbTe. Acta Mater. 2016, 111, 202−209.
(27) Xia, Y.; Hodges, J. M.; Kanatzidis, M. G.; Chan, M. K. Y. Lattice Thermal Transport in Group II-Alloyed PbTe. Appl. Phys. Lett. 2018, 112 (18), 181906.
(28) Horita, Z.; Ohashi, K.; Fujita, T.; Kaneko, K.; Langdon, T. G. Achieving High Strength and High Ductility in PrecipitationHardened Alloys. Adv. Mater. 2005, 17 (13), 1599−1602.
(29) Rogers, L. M. The Hall Mobility and Thermoelectric Power of P-Type Lead Telluride. Br. J. Appl. Phys. 1967, 18 (9), 1227.
(30) Luo, H.; Greene, R. G.; Ghandehari, K.; Li, T.; Ruoff, A. L. Structural Phase Transformations and the Equations of State of Calcium Chalcogenides at High Pressure. Phys. Rev. B: Condens. Matter Mater. Phys. 1994, 50 (22), 16232−16237.
(31) Kostryzhev, A.; Singh, N.; Chen, L.; Killmore, C.; Pereloma, E. Comparative Effect of Mo and Cr on Microstructure and Mechanical Properties in NbV-Microalloyed Bainitic Steels. Metals 2018, 8 (2), 134.
(32) Allgaier, R. S. Valence Bands in Lead Telluride. J. Appl. Phys. 1961, 32 (10), 2185−2189.

(33) Pei, Y.; Shi, X.; LaLonde, A.; Wang, H.; Chen, L.; Snyder, G. J. Convergence of Electronic Bands for High Performance Bulk Thermoelectrics. Nature 2011, 473 (7345), 66−69.
(34) Putley, E. H. The Hall effect and related phenomena, Semiconductor monographs; Butterworths: London, 1960.
(35) Zheng, L.; Li, W.; Lin, S.; Li, J.; Chen, Z.; Pei, Y. Interstitial Defects Improving Thermoelectric SnTe in Addition to Band Convergence. ACS Energy Lett. 2017, 2 (3), 563−568.
(36) Wang, X.; Veremchuk, I.; Bobnar, M.; Burkhardt, U.; Zhao, J.T.; Grin, Y. Sodium Substitution in Lead Telluride. Chem. Mater. 2018, 30 (4), 1362−1372.
(37) Tang, J.; Gao, B.; Lin, S.; Wang, X.; Zhang, X.; Xiong, F.; Li, W.; Chen, Y.; Pei, Y. Manipulation of Solubility and Interstitial Defects for Improving Thermoelectric SnTe Alloys. ACS Energy Lett. 2018, 3 (8), 1969−1974.
(38) Yang, J.; Meisner, G. P.; Chen, L. Strain Field Fluctuation Effects on Lattice Thermal Conductivity Of ZrNiSn-Based Thermoelectric Compounds. Appl. Phys. Lett. 2004, 85 (7), 1140−1142.
(39) Pei, Y.; Lensch-Falk, J.; Toberer, E. S.; Medlin, D. L.; Snyder, G. J. High Thermoelectric Performance in PbTe due to Large Nanoscale Ag2Te Precipitates and La Doping. Adv. Funct. Mater. 2011, 21 (2), 241−249.
(40) Ren, F.; Schmidt, R.; Keum, J. K.; Qian, B.; Case, E. D.; Littrell, K. C.; An, K. In Situ Neutron Scattering Study of Nanoscale Phase Evolution in PbTe-PbS Thermoelectric Material. Appl. Phys. Lett. 2016, 109 (8), 081903.
(41) Kim, H. S.; Liu, W.; Chen, G.; Chu, C.-W.; Ren, Z. Relationship between Thermoelectric Figure of Merit and Energy Conversion Efficiency. Proc. Natl. Acad. Sci. U. S. A. 2015, 112 (27), 8205−8210.
(42) Roychowdhury, S.; Panigrahi, R.; Perumal, S.; Biswas, K. Ultrahigh Thermoelectric Figure of Merit and Enhanced Mechanical Stability of p-type AgSb1−xZnxTe2. ACS Energy Lett. 2017, 2 (2), 349− 356.
(43) Kuna, R.; Adamiak, S.; Petit, S.; Baroni, P.; Gas, K.; Minikayev, R.; Szczerbakow, A.; Łazewski, J.; Szuszkiewicz, W. Hardening of (Pb,Cd)Te Crystal Lattice with an Increasing CdTe Content in the Solid Solution. Acta Phys. Pol., A 2016, 130, 1245−1247.
(44) Seidman, D. N.; Marquis, E. A.; Dunand, D. C. Precipitation Strengthening at Ambient and Elevated Temperatures of HeatTreatable Al(Sc) Alloys. Acta Mater. 2002, 50 (16), 4021−4035.
(45) Bhat, S. P.; Laird, C. High Temperature Cyclic Deformation of Precipitation Hardened Alloy · I. Partially Coherent Precipitates. Acta Metall. 1979, 27 (12), 1861−1871.